Originals

Experiments in Fluids 22 (1996) 1–13 © Springer-Verlag 1996

Velocity fidelity of flow tracer particles

R. Mei

Abstract Recent developments concerning the unsteady dynamic forces on a spherical particle at finite Reynolds number are reviewed for solid particles and clean micro-bubble. A particle frequency response function and an energy transfer function are derived for a solid particle or a contaminated micro-bubble in gas or liquid flow. A simple, unified method for estimating the cut-off frequency, or cut-off size, of a solid particle or a contaminated bubble is developed. Particle motion in isotropic turbulence is examined. Responses of the tracer particle to integral length scale structure, to turbulence energy, and to Taylor micro-scale structure are discussed in terms of the particle turbulence diffusivity, the particle turbulence intensity, and the ensemble average of the second invariant of fluid turbulence deformation tensor evaluated on the particle trajectory.

1 Introduction

In using modern optical techniques to measure fluid velocity field, such as laser Doppler velocimetry (LDV), particle image velocimetry (PIV), particle tracking velocimetry (PTV), and holographic particle image velocimetry (HPIV), tracer particles are seeded in flow fields that may be inherently three-dimensional and unsteady (Adrian 1991). Although different techniques are involved in obtaining the tracer particle velocity, it is commonly assumed that the tracer particle velocity equals to the local, instantaneous fluid velocity. While this is true in the limit of vanishing particle diameter (and inertia) the particle size in reality must always be finite, in order to obtain good quality optical signals. From this viewpoint, the following fundamental questions are sources of frequent concern in applying those optical techniques:

1) how well does the velocity of a tracer (or seed) particle of given size represent the unsteady fluid velocity?
2) how does one determine the largest possible size of the seed particles for a flow field of given time scales without affecting the velocity fidelity?

Since experimental conditions vary widely, it is not possible to give simple answers to those questions. The fluid may be liquid or gas and the seed particles may be solid, liquid droplets, or gas bubbles. The fluid velocity may range from micron per second to as high as $O(10^3)$ m/s. Interests in the flow field measurements may vary from large scale vortex structure to small scale structure on the order of Kolmogorov length scale.

In this paper, the issues raised above will be addressed by beginning with a detailed review of the recent development of particle dynamic equations for small and finite particle Reynolds number. Particle Reynolds number, *Re*, based on the slip velocity and particle diameter may be larger than one if particle size is large and the fluid velocity is highly turbulent. The frequency response of the seed particle will be subsequently examined. A criterion for determining particle size in terms of Stokes number and particle-to-fluid density ratio is suggested. The responses of the seed particle to turbulence structure on the integral length scale, to the turbulence energy, and to the Taylor micro-length scale structure are examined via a Monte-Carlo simulation of particle motion in a pseudo-turbulence and an analytical study (Mei and Adrian 1995). A simple asymptotic expression for predicting the energy loss of heavy fine particles due to small inertia in isotropic turbulence is derived. While the work in this paper is not experimental, *per se*, it is hoped that the experimentalists will find the results useful in designing and conducting fluid mechanical experiments.

Received: 13 November 1995/Accepted: 7 June 1996

R. Mei
Department of Aerospace Engineering
Mechanics and Engineering Science
University of Florida
Gainesville, FL 32611, USA

The author is grateful to R. J. Adrian and C. Kent for their encouragement and support in writing this paper. This work is supported by the Engineering Research Center (ERC) for Particle Science and Technology at the University of Florida, the National Science Foundation (EEC-9402989), and industrial partners of ERC.

2 Particle dynamics at finite Reynolds number

2.1 Unsteady drag on a solid particle at zero Reynolds number

The earliest work related to the unsteady drag on a spherical particle was that of Stokes (1851) and Basset (1888). Their results were derived in the frequency and time domains, respectively, in the creeping flow limit. For a sphere of radius a moving through stationary fluid of viscosity μ and density ρ_f with unidirectional velocity $V(t)$, Basset obtained the following expression for the hydrodynamic force on particle at zero Reynolds number,

$$F(t) = -6\pi\mu a V(t) - 6\pi\mu a^2 \int_{-\infty}^{t} \frac{dV}{d\tau} \frac{d\tau}{\sqrt{\pi\nu(t-\tau)}} - \frac{2}{3}\pi a^3 \rho_f \frac{dV}{dt}$$

$$= F_{QS}(t) + F_H(t) + F_{AM}(t) \qquad (1)$$

where ν is the fluid kinematic viscosity. The first term, $F_{QS}(t)$, is a quasi-steady viscous force. The second term, $F_H(t)$, is called the history force or Basset force. It is due to the diffusion of the vorticity from the particle surface to the bulk fluid flow. The third term, $F_{AM}(t)$, is the added-mass force which is purely inertial. If the frame of reference is fixed with the sphere and the fluid moves with a uniform velocity $U(t)$ in a far field over a stationary sphere, the force is

$$F(t) = 6\pi\mu a U(t) + 6\pi\mu a^2 \int_{-\infty}^{t} \frac{dU}{d\tau} \frac{d\tau}{\sqrt{\pi\nu(t-\tau)}}$$

$$+ \frac{2}{3}\pi a^3 \rho_f \frac{dU}{dt} + \frac{4}{3}\pi a^3 \rho_f \frac{dU}{dt} \qquad (2)$$

The first three terms are the same as in Eq. (1). The last term, $\frac{4}{3}\pi a^3 \rho_f (dU/d\tau)$, is the product of the acceleration and the fluid mass displaced by the particle; it results from the coordinate transformation since the frame of reference of the particle is non-inertial.

Tchen (1947) proposed an equation of motion for particles moving in an unsteady non-uniform flow in a form that essentially combines the above two equations in an *ad hoc* manner. A more rigorous derivation of the equation of motion for small spherical particles of density ρ_p at zero particle Reynolds number was given by Maxey and Riley (1983) in the form of

$$\frac{4}{3}\pi a^3 \rho_p \frac{d\mathbf{V}}{dt} = \frac{4}{3}\pi a^3 (\rho_p - \rho_f)\mathbf{g} - 6\pi\mu a \left(\mathbf{V} - \mathbf{U} - \frac{1}{6} a^2 \nabla^2 \mathbf{U}\right)$$

$$- 6\pi\mu a^2 \int_{t_0}^{t} \frac{d}{d\tau}\left(\mathbf{V} - \mathbf{U} - \frac{1}{6} a^2 \nabla^2 \mathbf{U}\right) \frac{d\tau}{\sqrt{\pi\nu(t-\tau)}}$$

$$- \frac{2}{3}\pi a^3 \rho_f \frac{d}{dt}\left(\mathbf{V} - \mathbf{U} - \frac{1}{10} a^2 \nabla^2 \mathbf{U}\right) + \frac{4}{3}\pi a^3 \rho_f \frac{D\mathbf{U}}{Dt}$$

$$= \mathbf{F}_{G-B} + \mathbf{F}_{QS}(t) + \mathbf{F}_H(t) + \mathbf{F}_{AM}(t) + \mathbf{F}_{FS}(t) \qquad (3)$$

where $\mathbf{V}$ and $\mathbf{U}$ are the velocities of the particle and the fluid and $\mathbf{g}$ is the gravitational acceleration. The first term, $\mathbf{F}_{G-B}$, is the body force (gravity minus buoyancy). Here, d/dt refers to the time derivative on the particle trajectory and can be evaluated as $(\partial/\partial t + \mathbf{V}\cdot\nabla)$ and $D/Dt = \partial/\partial t + \mathbf{U}\cdot\nabla$ refers to the time derivative evaluated on the trajectory of the fluid elements that surrounds the particle at any given instant. The Faxen terms, $a^2\nabla^2\mathbf{U}$, in (3) are normally small in comparison with any of the remaining terms, and so they can be neglected. The last term in (3), $\mathbf{F}_{FS}(t) = \frac{4}{3}\pi a^3 \rho_f (D\mathbf{U}/Dt)$, includes the last term in Eq. (2), $\frac{4}{3}\pi a^3 \rho_f (\partial\mathbf{U}/\partial t)$. The derivation of Eq. (3) can be briefly summarized as follows. Consider a spherical particle introduced at $\mathbf{x} = \mathbf{x}_p$ with a velocity $\mathbf{V}$ into an otherwise undisturbed non-uniform flow field of velocity $\mathbf{U}(t, \mathbf{x})$ and stress field $\boldsymbol{\sigma}^0$. The flow field around the sphere is modified to be $\mathbf{u}(t, \mathbf{x})$ with $\mathbf{u}(t, \mathbf{x}) = \mathbf{V}$ on the particle surface S defined by $|\mathbf{x} - \mathbf{x}_p| = a$, and $\mathbf{u}(t, \mathbf{x}) \to \mathbf{U}(t, \mathbf{x})$ as $|\mathbf{x} - \mathbf{x}_p| \to \infty$. The resulting stress field can be expressed as $\boldsymbol{\sigma} = \boldsymbol{\sigma}^0 + \boldsymbol{\sigma}'$ in which $\boldsymbol{\sigma}'$ is the disturbance stress field and is related to the relative velocity $(\mathbf{V} - \mathbf{U})$. While the hydrostatic pressure gives rise to $\mathbf{F}_{G-B}$, $\oiint_S \mathbf{n}\cdot\boldsymbol{\sigma}'\, dS$ contributes to $\mathbf{F}_{QS}(t)$, $\mathbf{F}_H(t)$, and $\mathbf{F}_{AM}(t)$ in Eq. (3), and the contribution from $\boldsymbol{\sigma}^0$ becomes $\mathbf{F}_{FS}(t) = \oiint_S \mathbf{n}\cdot\boldsymbol{\sigma}^0\, dS \sim \frac{4}{3}\pi a^3 \nabla\cdot\boldsymbol{\sigma}^0 = \frac{4}{3}\pi a^3 \rho_f (D\mathbf{U}/Dt)$ by using the divergence theorem and Navier–Stokes equation for the undisturbed flow field, $\rho_f (D\mathbf{U}/Dt) = \nabla\cdot\boldsymbol{\sigma}^0$.

It should be noted that the added-mass force described by (3) is proportional to $(d/dt)(\mathbf{V} - \mathbf{U})$. However, based on an analysis of inviscid non-uniform flow over a sphere, Auton et al. (1988) have shown that added-mass force on a sphere *in general* should be expressed as

$$\mathbf{F}_{AM}(t) = \frac{2}{3}\pi a^3 \rho_f \left(\frac{D\mathbf{U}}{Dt} - \frac{d\mathbf{V}}{dt}\right) \qquad (4)$$

Since in the derivation of Eq. (3) by Maxey and Riley, the nonlinear convection term in the Navier–Stokes equation governing the relative motion between the particle and the surrounding fluid was not included, the difference, $D\mathbf{U}/Dt - d\mathbf{U}/dt = (\mathbf{U} - \mathbf{V})\cdot\nabla\mathbf{U}$ does not appear in the equation, and it has no tangible impact on the accuracy of Eq. (3) within the low Reynolds number approximation. At finite Reynolds number, this is no longer true, and the correction of Auton et al. (1988) should be incorporated into Maxey–Riely's equation. However, for typical seed particles having reasonably small inertia, $|\mathbf{U} - \mathbf{V}| \ll |\mathbf{U}|$ in order for the measurement error to be small. Thus the difference $(\mathbf{U} - \mathbf{V})\cdot\nabla\mathbf{U}$ is quite small compared with the typical term $\mathbf{U}\cdot\nabla\mathbf{U}$ in $D\mathbf{U}/Dt$ and Eq. (3) can be used in unmodified form. It is also noted that this difference vanishes when a particle is in a uniform flow.

2.2 Unsteady drag on a solid particle at finite Reynolds number

Let L be a characteristic length of the flow field and a usual flow Reynolds number is defined as $Re_L = UL/\nu$ in which U is a characteristic velocity. Defining particle Reynolds number as

$$Re = |\mathbf{U} - \mathbf{V}|2a/\nu \qquad (5)$$

the small error requirement, $|\mathbf{U} - \mathbf{V}|/|\mathbf{U}| \ll 1$, implies that $Re(\nu/a|\mathbf{U}|) \ll 1$. This is equivalent to $(Re/Re_L)L/a \ll 1$ or $Re \ll (a/L)Re_L$ by using U as an estimate for $|\mathbf{U}|$. Ordinarily, a/L is very small. In PIV measurement of a liquid flow, $a \sim 10$ μm and $L \geqslant 10$ mm so that $a/L \sim 10^{-3}$. In an air flow, $a \sim 1$ μm and $L \geqslant 10$ mm so that $a/L \sim 10^{-4}$. Thus one requires $Re \ll 10^{-3} - 10^{-4} Re_L$. If the flow is laminar, typically $Re_L < 10^3$ and $Re \ll 1$ can be satisfied. If the flow is turbulent, $Re_L > 10^3$ permits $Re > 1$ with small measurement error. Thus for laminar flow we can use the low Reynolds number Eq. (3) to study the particle motion. For turbulent flows, a finite Reynolds number particle dynamic equation is needed to adequately describe the particle motion.

2.2.1 On the quasi-steady force

There have been various attempts to extend Tchen's or Maxey and Riley's equation to particle Reynolds number of order unity or larger. A common approach, often adopted in many books and papers in the literature, is to consider the quasi-steady force and simply neglect the unsteady forces $F_H(t)+F_{AM}(t)+F_{FS}(t)$. The quasi-steady force is usually represented by using the steady-state drag coefficient with instantaneous velocities $(\mathbf{U}-\mathbf{V})$,

$$\mathbf{F}_{QS}=6\pi\mu a\phi(\mathbf{U}-\mathbf{V}) \tag{6}$$

where ϕ accounts for the deviation from the Stokes drag when the Reynolds number becomes finite. A commonly used expression for ϕ is (Clift et al. 1978)

$$\phi=(1+0.15Re^{0.687}) \tag{7a}$$

and more accurate forms compiled by Clift et al. (1978) are

$$\phi=1+\frac{3}{16}Re, \qquad Re\leqslant 0.01 \tag{7b}$$

$$=1+0.1315Re^{0.82-0.05w},\ w=\log_{10}Re, \qquad 0.01<Re\leqslant 20 \tag{7c}$$

$$=1+0.1935\,Re^{0.6305}, \qquad 20<Re\leqslant 260 \tag{7d}$$

2.2.2 On the added-mass force and history force

The neglect of the unsteady forces is not always justified. For a solid particle in liquid, the unsteady forces can be significant with moderate acceleration (Clift et al. 1978, p. 286). Odar and Hamilton (1964) and Odar (1966) performed carefully controlled experiments to measure the unsteady drag on an oscillating sphere in a stagnant oil tank for $Re<62$, and they proposed modifications for $F_H(t)$ and $F_{AM}(t)$ based on an acceleration parameter. Schöneborn (1975), Karanfilian and Kotas (1978), Clift et al. (1978, p. 296), Tsuji et al. (1991), and Linteris et al. (1991) adopted the approach of Odar and Hamilton to correlate their experimentally measured unsteady forces using the acceleration parameter.

However, the modifications of the history force and the added-mass force due to Odar and Hamilton (1964) are not physically sound because they do not give correct long-time asymptotic decay of the history force, and they do not approach Stokes' (1851) solution for an arbitrary acceleration as $Re\to 0$. The expression for the history force proposed by Odar and Hamilton (1964) and Odar (1966) has the same integration kernel as the creeping flow approximation, and it is not valid at non-zero Re. Furthermore, the experiments were conducted only for several discrete frequencies, which are relatively high and do not cover the entire frequency domain. Mei (1993) compared Odar and Hamilton's expression for $F_H(t)$ with the finite difference solution for the transient force when the particle is impulsively started and a constant velocity is subsequently maintained. It was shown that Odar and Hamilton's (1964) empirical expression under-predicts the short time history force by over 50%, and it significantly over-predicts the long-time history force.

Mei et al. (1991) computed the unsteady force on a stationary sphere in a flow with a large mean free-stream velocity and a small fluctuation by solving the unsteady Navier–Stokes equation in the frequency domain. They deduced the added-mass force from the imaginary part of the unsteady drag in the high frequency limit at finite Re, based on the numerical results. It was demonstrated that the force due to the added mass at finite Re, is the same as in creeping flow ($Re\to 0$) and in potential flow. Note that in this problem $\mathbf{V}=0$ and $\nabla\mathbf{U}=0$ so $\mathbf{F}_{AM}=\frac{2}{3}\pi a^3\rho_f\,(\mathrm{D}\mathbf{U}/\mathrm{D}t)$ is the same as in (3), derived in the creeping flow limit. The findings about the added-mass force cited in the review by Torobin and Gauvin (1959), which stated that, "The added mass concept is shown to be both completely inadequate and theoretically unsound", are simply incorrect. *No correction* is needed for the added-mass force at finite Reynolds number since it is a purely inertial effect independent of viscosity. Rivero et al. (1991) carried out a numerical procedure to separate the contributions to the total unsteady force from the history force and the instantaneous added-mass force. The analysis of an oscillating flow and a uniformly accelerating flow demonstrated that the added-mass force is the same as in potential flow. The recent simulations for oscillatory motion and linear acceleration (Chang and Maxey 1994, 1995) in the time domain also support this conclusion. For finite Reynolds number particle dynamics, Eq. (4) is thus used for the added-mass force.

2.2.3 A proposed particle dynamic equation at finite *Re*

Using the results of a numerical analysis at finite Re over a wide range of frequencies from Mei et al. (1991), an asymptotic analysis at small Re and low frequency, the principle of causality, and an interpolation for the imaginary component of the history force in the frequency domain, Mei and Adrian (1992) modified the history force kernel for a sphere experiencing a large mean free-stream velocity with a small fluctuation. The important result from this study is that the history force kernel recovers the $(t-\tau)^{-1/2}$ behavior at small times, but it possesses a $(t-\tau)^{-2}$ decay at large time, as opposed to the $(t-\tau)^{-1/2}$ decay derived by Basset (1888). This $(t-\tau)^{-2}$ long-time decay results from retaining the nonlinear convection terms in the Navier–Stokes equation; it is consistent with the result of Sano (1981). The realization that the history force kernel decays rapidly at large time resolves the paradox of Reeks and Mckee (1984), wherein the initial velocity difference between the particle and the fluid makes a finite contribution to the particle long time diffusivity.

Using the history force expression proposed in Mei and Adrian (1992) for the case of a large mean free-stream velocity with a small fluctuation, and the expression for the added-mass force by Auton et al. (1988), Mei (1994) proposed the following dynamic equation to describe the uni-directional motion of spherical particles at *finite* Reynolds number,

$$\begin{aligned}\frac{4}{3}\pi a^3\rho_p\frac{\mathrm{d}V}{\mathrm{d}t}&=\frac{4}{3}\pi a^3(\rho_p-\rho_f)g+6\pi\mu a\phi(Re)\,(U-V)\\&\quad+6\pi\mu a\int_{t_0}^{t}K(t-\tau)\,\frac{\mathrm{d}(U-V)}{\mathrm{d}\tau}\,\mathrm{d}\tau\\&\quad+\frac{2}{3}\pi a^3\rho_f\left(\frac{\mathrm{D}U}{\mathrm{D}t}-\frac{\mathrm{d}V}{\mathrm{d}t}\right)+\frac{4}{3}\pi a^3\rho_f\,\frac{\mathrm{D}U}{\mathrm{D}t}\end{aligned} \tag{8}$$

where $\phi(Re)$ is given by Eq. (7). The history force kernel $K(t-\tau)$ is approximated as

$$K(t-\tau) \approx \left\{ \left[\frac{\pi(t-\tau)\nu}{a^2} \right]^{1/4} + \left[\frac{\pi}{2} \frac{|U(\tau)-V(\tau)|^3}{a\nu f_H^3(Re)} (t-\tau)^2 \right]^{1/2} \right\}^{-2} \tag{9}$$

with

$$f_H(Re) = 0.75 + 0.105 Re \tag{10}$$

For a particle introduced to the flow field at $x = x_0$ at time $t = t_0$ with an initial velocity V_0 different from the local fluid velocity $U_0 = U(t_0, x_0)$, the lower limit of the integration in (8) is t_0^- (Mei 1993), the instant right before the particle is introduced. Thus the history force term can be further expanded as

$$F_H = 6\pi\mu a \int_{t_0^+}^{t} K(t-\tau) \frac{\mathrm{d}(U-V)}{\mathrm{d}\tau} \mathrm{d}\tau + 6\pi\mu a (U_0 - V_0) K_0(t) \tag{11}$$

where t_0^+ is the instant right after the particle is introduced, and $K_0(t)$ is the kernel based on the velocity difference at $t = t_0$. For two- or three-dimensional flows, Eq. (8) may be generalized to a vector form; but much remains to be investigated.

Equation (8) is only an approximation, since $K(t-\tau)$ was developed in an approximate manner. Several tests have been performed (Mei 1994) to examine the accuracy and the validity of Eqs. (8–10) against numerical and experimental results. These tests include:

i) a purely oscillating sphere in a stagnant liquid using the numerical results of Mei (1994) and the experimental results of Odar and Hamilton (1964);
ii) a large mean free-stream velocity with a small fluctuation passing a sphere based on the numerical results of Mei et al. (1991);
iii) a sphere that possesses a large terminal velocity settling in a stagnant viscous liquid with initially zero velocity based on measurements of Moorman (1955).

Comparisons were made for each force component in addition to the total drag. The test results indicate that, when the unsteady forces are not negligible, Eqs. (8–10) are reliable, robust, accurate at small time, and qualitatively correct at large times over a large range of Reynolds number. It is easily seen that Eqs. (7–10) reduces to (3) as $Re \to 0$ except for $F_{AM}(t)$ where the more correct form given by Eq. (4) is used. Thus, Eqs. (7–10) may be used for $Re < 173$. Beyond this value the three-dimensional instability will develop (Kim and Perlstein 1990).

Mei (1993) and Lawrence and Mei (1995) further considered an unsteady flow due to a step change in the velocity of a sphere from $U = U_1 \geqslant 0$ to $U = U_2 > 0$. The transient force was obtained using a finite difference method for finite Re over a large range of time. The history force on the sphere could be obtained by subtracting the steady drag from the computed total drag because $F_{AM}(t)$ and $F_{FS}(t)$ vanish for $t > 0$. For such a singular acceleration, the numerical results indicate that the approximate expressions (9–10) give the correct short time behavior for the history force and capture qualitatively its long-time behavior for finite Re. Most importantly, the asymptotic and numerical results of Lawrence and Mei (1995) have convincingly shown that the history force associated with the step change in the velocity (from $U_1 \geqslant 0$ to $U_2 > 0$) decays as t^{-2} at large time which supports the qualitative long-time behavior of $F_H(t)$ given by equations (9–10). This t^{-2} long-time decay of the transient force at finite Re for the case of a sudden change in the particle velocity from $U_1 > 0$ to $U_2 > 0$ is also in excellent agreement with a more recent, and a more accurate, low-Reynolds-number analytical result by Lovalenti and Brady (1995). Mei and Lawrence (1996) also give detailed asymptotic and numerical analyses for the flow field associated with the sudden change in the velocity which support the t^{-2} long-time decay of the transient force.

However, because of its approximate nature, there are several extreme cases for which Eq. (9) cannot describe the long-time history force correctly. They are: i) a particle stops impulsively; and ii) a particle reverses impulsively. In those two cases, the long-time decay of the transient force is t^{-1} instead of t^{-2} due to the fact that the particle encounters the laminar far-wake it created earlier (Lawrence and Mei 1995; Mei and Lawrence 1996). For a sphere oscillating at low frequency, it was also pointed out (Mei 1994) that the imaginary part of the history force D_{IH} exhibits a $-\omega \log \omega$ dependence on frequency ω, as opposed to $D_{IH} \sim \omega$ for the case of a large mean free-stream velocity with a small fluctuation. In a strict sense, Eq. (9) thus fails to capture this low frequency $\omega \log \omega$ behavior. Nevertheless, those impulsive accelerations for particle motions are rare and the history force at low oscillation frequency is of a small magnitude in comparison with the quasi-steady drag.

Lovalenti and Brady (1993a, b) used a reciprocal theorem and Oseen's point force to develop a complicated, but more accurate, expression for hydrodynamic force at *low Reynolds number*,

$$\begin{aligned} \mathbf{F}(t) &= 6\pi\mu a \mathbf{u}(t) + 6\pi\mu a \frac{3}{8} \sqrt{\frac{a^2}{\pi\nu}} \\ &\times \int_{-\infty}^{t} \left\{ \frac{2}{3} \mathbf{u}^{\parallel}(t) - \left[\frac{1}{A^2} \left(\frac{\pi^{1/2}}{2A} \operatorname{erf}(A) - \mathrm{e}^{-A^2} \right) \right] \mathbf{u}^{\parallel}(\tau) \right. \\ &\left. + \frac{2}{3} \mathbf{u}^{\perp}(\tau) - \left[\mathrm{e}^{-A^2} - \frac{1}{2A^2} \left(\frac{\pi^{1/2}}{2A} \operatorname{erf}(A) - \mathrm{e}^{-A^2} \right) \right] \mathbf{u}^{\perp}(\tau) \right\} \\ &\times \frac{2\mathrm{d}\tau}{(t-\tau)^{3/2}} + \frac{2}{3} \pi a^3 \rho_f \dot{\mathbf{u}}(t) + \frac{4}{3} \pi a^3 \rho_f \frac{\mathrm{D}\mathbf{U}}{\mathrm{D}t} \end{aligned} \tag{12}$$

where $\mathbf{u}(t) = \mathbf{U}(t) - \mathbf{V}(t)$, A relates to the magnitude of the relative displacement between time τ and t,

$$A(t,\tau) = |\mathbf{A}(t,\tau)| = \frac{1}{2} \frac{1}{\sqrt{\nu(t-\tau)}} \left| \int_{\tau}^{t} -\mathbf{u}(s)\,\mathrm{d}s \right| \tag{13}$$

and $\mathbf{u}^{\parallel}(\tau)$, $\mathbf{u}^{\perp}(\tau)$ are the components of the relative velocity at time τ, respectively parallel and perpendicular to the displacement vector $\mathbf{A}(t,\tau)$. While the above equation is valid for numerous cases of unsteady particle motion, the long-time behavior of the transient force due to a sudden change in the particle (or fluid) velocity in the same direction is not correctly predicted (Lawrence and Mei 1995; Lovalenti and Brady 1995); Eq. (12) gives an exponential decay of the transient force rather than t^{-2} decay. For an oscillating flow over a stationary particle, it was shown (Mei 1994) that the prediction based on Eq. (12) gives excellent agreement with the numerical solution of the Navier–Stokes equation at *low Reynolds number*. Hence Eq. (12) is accurate and useful in most cases when particle Reynolds number is less than one.

2.2
Unsteady drag on bubbles in a unidirectional motion at finite Reynolds number

Depending on the extent of the contamination of the liquid, a bubble may behave as a *rigid particle* if the liquid/gas interface is immobile, or as a *clean bubble* that exhibits a high interfacial mobility (or zero shear stress) on the interface if the effect of surfactant is negligible. In most bubbly flows, there is sufficient contaminant in a natural liquid environment to suppress the liquid/gas interface mobility. If the bubble size is not large, the surface tension force is able to keep the bubble in spherical shape. For droplets and micro-bubbles with an immobile interface, the dynamic equations are the same as for solid particles. Hence, Eqs. (7–10) can be used to describe the motion of contaminated micro bubbles in unsteady flows.

For clean spherical bubbles, the steady drag is $\frac{2}{3}$ of that on a rigid particle in the creeping flow regime. Brabston (1974) numerically obtained the steady drag for the range $Re=0.1$–60. For unsteady motions, the history force also exists on a clean bubble besides the quasi-steady force and the added-mass force (Auton et al. 1988; Drew and Layhey 1990), as was demonstrated in Chen (1970), Sy et al. (1970), Kim and Krilla (1991), Yang and Leal (1991), Mei and Klausner (1992), Lovalenti and Brady (1993b), and Mei et al. (1994). While Lovalenti and Brady's (1993b) equation for the unsteady force on a fluid bubble or drop is accurate, it is only applicable for $Re<1$. For finite Reynolds number, Mei et al. (1994) developed an approximate expression for the total force on a clean bubble executing a rectilinear motion which can be symbolically given as

$$\frac{4}{3}\pi a^3\rho_b\frac{\mathrm{d}V}{\mathrm{d}t}=F_{B-G}+F_{QS}(t)+F_H(t)+F_{AM}(t)+F_{FS}(t) \qquad (13)$$

where F_{B-G}, $F_{AM}(t)$, and $F_{FS}(t)$ are identical to those on solid particles. The quasi-steady force on the clean bubble is given by

$$F_{QS}(t)=6\pi\mu a(U-V)\left\{\frac{2}{3}+\left[\frac{12}{Re}+0.75\left(1+\frac{3.315}{Re^{1/2}}\right)\right]^{-1}\right\} \qquad (14)$$

The history force F_H is also expressed as $6\pi\mu a\int_{t_0}^{t}K(t-\tau)\times[\mathrm{d}(U-V)/\mathrm{d}\tau]\,\mathrm{d}\tau$. The expression for the kernel $K(t-\tau)$ that approximates both small time and large time behavior correctly is lengthy and can be found in Mei et al. (1994). In the solid sphere case, the history-force kernel at small time is given as $K(t-\tau)\approx[\pi(t-\tau)v/a^2]^{-1/2}$. The kernel for a clean bubble at small time, $K(0)$, is finite valued and decreases with increasing Re. For an impulsively started flow over a bubble, accurate finite difference results show that the history force on the bubble decays as t^{-2} at large time. Satisfactory agreement was observed between the proposed history force and the numerical solution for the impulsively started bubble.

Park et al. (1995, 1996) obtained accurate measurements of the trajectories of spherical bubbles rising in a clean, stagnant liquid. The terminal Reynolds number and Weber number ranged from 6 to 212 and 0.03 to 0.69, respectively. The agreement between the measurement and the prediction using the approximate expression for the history force $F_H(t)$ on a clean bubble proposed by Mei et al.(1994) for finite Re was excellent. Hence the approximate expression for $F_H(t)$ was validated for rising bubbles in a clean, stagnant liquid. It was also demonstrated that neglecting $F_H(t)$ resulted in a discernible over-prediction for the bubble trajectory. Using the creeping flow result for $F_H(t)$ could lead to a significant under-prediction for the trajectory at large Re due to the over-prediction in $F_H(t)$.

In strong shear flows, the effects of shear lift force (Saffman 1965, 1968) and Magnus force (Rubinow and Keller 1961) add another dimension of complexity to the particle dynamic equation at finite Re. The shear lift force is important if the shear rate and the slip velocity between particles and fluid are both large. While the interaction between the lift force and unsteadiness in the translational motion of the particle is not clear, recent experimental and computational works by Tsuji et al. (1985), Dandy and Dwyer (1990), McLaughlin (1991), Mei and Klausner (1994), Sridhar and Katz (1995), Cherukat et al. (1995) shed further light on the complex behavior of the lift force at finite Reynolds number.

3
Particle frequency response function and cut-off frequency

3.1
Response function in the high frequency (ω) limit

In determining the response of seed particles to the unsteady fluid velocity, it is the high-frequency part of the spectrum that is of interest. If a particle can follow the high frequency fluctuation, it can certainly follow the lower frequency fluctuation better. To this end, we first consider the unsteady drag on a stationary sphere of radius a experiencing a high-frequency (ω) rectilinear oscillation of the fluid flow,

$$u(t)=\tilde{u}(\omega)\,\mathrm{e}^{-\mathrm{i}\omega t} \qquad (15)$$

in which $\tilde{u}(\omega)$ is the amplitude of the fluid velocity oscillation. The Reynolds number $Re=\tilde{u}2a/v$ is finite. Defining a Stokes number

$$\varepsilon=\sqrt{\omega a^2/2v}\gg 1 \qquad (16)$$

asymptotic analysis (Mei 1994) gives the following form of the unsteady drag on the sphere at finite Re,

$$F/[6\pi\mu a\tilde{u}(\omega)]\sim\mathrm{e}^{-\mathrm{i}\omega t}\left[-\frac{2}{3}\mathrm{i}\varepsilon^2+\varepsilon(1-\mathrm{i})+1\right],\quad \varepsilon\gg 1 \qquad (17)$$

In the above $-\frac{2}{3}\mathrm{i}\varepsilon^2\mathrm{e}^{-\mathrm{i}\omega t}$ results from $F_{AM}/[6\pi\mu a\tilde{u}(\omega)]=-\frac{2}{9}\mathrm{i}\varepsilon^2\mathrm{e}^{-\mathrm{i}\omega t}$ and $F_{FS}/[6\pi\mu a\tilde{u}(\omega)]=-\frac{4}{9}\mathrm{i}\varepsilon^2\mathrm{e}^{-\mathrm{i}\omega t}$. The history force gives the contribution $\varepsilon(1-\mathrm{i})\mathrm{e}^{-\mathrm{i}\omega t}$ in Eq. (17). The quasi-steady force is $\mathrm{O}(1)$ at large ε. It should be pointed out that although $\varepsilon\gg 1$ is required in the asymptotic analysis at finite Re, Eq. (17) becomes exact for $Re\ll 1$, and it is quite accurate for ε near one when Re is less than 20. When the particle is allowed to respond to this oscillating flow field, it can be easily shown with the aid of Eq. (17) that Eq. (8) can be cast in the form of

$$-\mathrm{i}\omega\frac{4}{3}\pi a^3\rho_p\tilde{v}(\omega)\mathrm{e}^{-\mathrm{i}\omega t}\sim 6\pi\mu a(\tilde{u}-\tilde{v})\mathrm{e}^{-\mathrm{i}\omega t} + 6\pi\mu a(1-\mathrm{i})\varepsilon(\tilde{u}-\tilde{v})\mathrm{e}^{-\mathrm{i}\omega t} + \mathrm{i}\omega\frac{2}{3}\pi a^3\rho_f\tilde{v}(\omega)\mathrm{e}^{-\mathrm{i}\omega t} - \mathrm{i}\omega 2\pi a^3\rho_f\tilde{u}(\omega)\mathrm{e}^{-\mathrm{i}\omega t} \qquad (18)$$

It is noted that since the particle dynamic equation for the contaminated micro-bubble is the same as for solid particles, the above equation is also valid when $\rho_p\to 0$. Let the particle-to-fluid density ratio be

$$\rho=\rho_p/\rho_f \qquad (19)$$

and a particle inertia parameter (whose inverse is a particle response time) be

$$\beta=\frac{9}{2}\frac{\nu}{(\rho+1/2)a^2} \qquad (20)$$

Then, the particle velocity amplitude $\tilde{v}(\omega)$ can be expressed as

$$\tilde{v}(\omega)\sim\frac{1+\varepsilon-\mathrm{i}\varepsilon-\mathrm{i}[3\omega/(2\rho+1)\beta]}{1+\varepsilon-\mathrm{i}\varepsilon-\mathrm{i}\omega/\beta}\tilde{u}(\omega) \qquad (21a)$$

or

$$\tilde{v}(\omega)\sim\frac{1+\varepsilon-\mathrm{i}\varepsilon-\mathrm{i}\frac{2}{3}\varepsilon^2}{1+\varepsilon-\mathrm{i}\varepsilon-\mathrm{i}\frac{4}{9}(\rho+\frac{1}{2})\varepsilon^2}\tilde{u}(\omega)=H(\omega)\tilde{u}(\omega) \qquad (21b)$$

where $H(\omega)$ is *frequency response function* of the particle. It is important to note that the only parameter in Eq. (21b) is the particle-to-fluid density ratio ρ because the particle inertia is embedded in the Stokes number. The *energy transfer function* at for arbitrary ε with small Re or asymptotically large ε with finite Re is

$$|H(\omega)|^2=|H(\varepsilon)|^2=\frac{(1+\varepsilon)^2+(\varepsilon+\frac{2}{3}\varepsilon^2)^2}{(1+\varepsilon)^2+[\varepsilon+\frac{2}{3}\varepsilon^2+\frac{4}{9}(\rho-1)\varepsilon^2]^2} \qquad (22)$$

Figure 1 shows the dependence of $|H(\varepsilon)|^2$ on the Stokes number ε over a wide range of density ratio ρ. The following observations are worth noting.

i) For a neutrally buoyant particle, $\rho=1$, and $|H(\varepsilon)|^2=1$, which implies *perfect response* of the seed particle.
ii) At $\rho=0$, $|H(\varepsilon)|^2\to 9$ as $\varepsilon\to\infty$ which suggests a significant over-shoot at high frequency.
iii) For $\rho<1$, $|H(\varepsilon)|^2>1$ so that buoyant particles tend to over-respond.
iv) For $\rho\gg 1$, $|H(\varepsilon)|^2\to\frac{81}{16}\rho^{-2}\varepsilon^{-4}$ at intermediate ε. This implies a low-pass filtering behavior of heavy particles; at large ε, $|H(\varepsilon)|^2\to\frac{9}{4}\rho^{-2}$ which implies practically negligible frequency response.

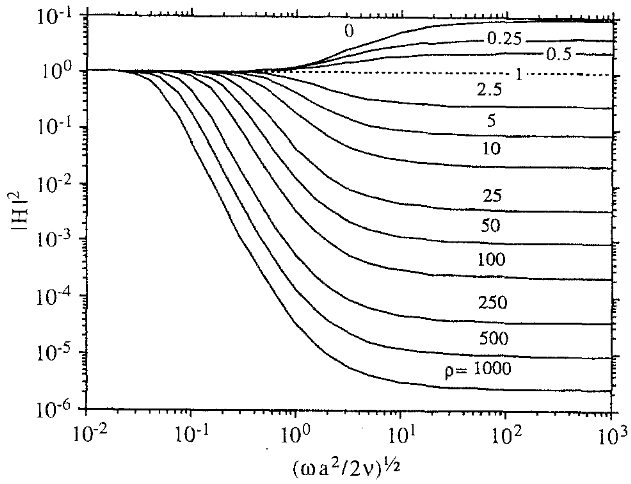

Fig. 1. Particle energy transfer function $|H(\varepsilon)|^2$ as a function of Stokes number ε

3.2
Cut-off frequency for solid particle and contaminated bubble

Define cut-off frequencies of the particle based on either 50% or 200% energy response,

$$\varepsilon_{\text{cut-off}}=\{\varepsilon:\ |H(\varepsilon)|^2=\tfrac{1}{2}\ \text{or}\ 2\}. \qquad (23)$$

Then $\varepsilon_{\text{cut-off}}$ can be obtained as a function of ρ from Eq. (22). Figure 2 shows the dependence of $\varepsilon_{\text{cut-off}}$ on ρ. The following can be observed easily.

i) For $0.56\leqslant\rho\leqslant 1.62$, $0.5<|H|^2<2$ implying very good response of the seed particle.
ii) For a solid particle in air, reducing ρ alone from 1000 to 100, say by using a hollow sphere, will only increase $\omega_{\text{cut-off}}$ by a factor of $\sqrt{10}=3.16$.
iii) At a given ρ, decreasing the particle diameter by a factor of 10 will increase $\omega_{\text{cut-off}}$ by a factor of 100 since $\omega_{\text{cut-off}}=2\nu(\varepsilon_{\text{cut-off}}/a)^2$.

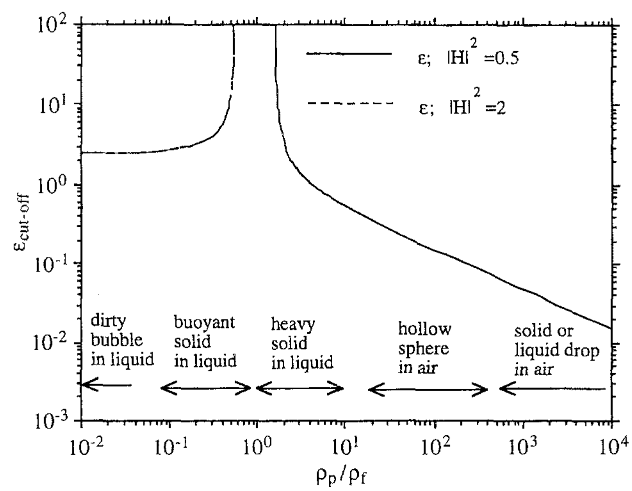

Fig. 2. Cut-off Stokes number as a function of particle-to-fluid density ratio

For convenience, the following interpolation formulae are provided to estimate $\varepsilon_{\text{cut-off}}$

$$\varepsilon_{\text{cut-off}} \approx \left[2.380^n + \left(\frac{0.659}{0.561-\rho} - 1.175\right)^n\right]^{1/n}, \quad n=0.93 \quad \text{for } \rho<0.561 \quad (24a)$$

$$\varepsilon_{\text{cut-off}} \approx \left[\left(\frac{3}{2\rho^{1/2}}\right)^\gamma + \left(\frac{0.932}{\rho-1.621}\right)^\gamma\right]^{1/\gamma}, \quad \gamma=1.05, \quad \text{for } \rho>1.621 \quad (24b)$$

Using

$$f_{\text{cut-off}} \approx \frac{\nu}{\pi}\left(\frac{\varepsilon_{\text{cut-off}}}{a}\right)^2 \quad (25)$$

the cut-off frequency of the seed particle can be easily determined. For example, for a droplet in air with $\rho=813$ and $\nu=0.15$ cm^2/s, one obtains $\varepsilon_{\text{cut-off}} \approx 0.0535$ from (24b). For 0.5 μm $<a<$ 5 μm, the cut-off frequency $f_{\text{cut-off}} \approx \nu/\pi(\varepsilon_{\text{cut-off}}/a)^2$ ranges from 54.7 kHz to 547 Hz. For phenolic micro-balloons (or hollow spheres) in air with particle size in the range of $a=15$–25 μm, the particle effective density ranges from 100–500 kg/m^3, which gives the density ratio ranging from 81.3 to 406.5. It is estimated that $\varepsilon_{\text{cut-off}} \approx 0.176$ to 0.0762. The cut-off frequencies range between 658–237 Hz and 123–44.4 Hz, respectively for $\rho_p=100$ kg/m^3 and $\rho_p=500$ kg/m^3. For contaminated bubbles in a liquid of viscosity $\nu=0.01$ cm^2/s, $\varepsilon_{\text{cut-off}} \approx 2.38$. If the bubble radius ranges from 5 to 25 μm, the cut-off frequency then ranges from 72 to 2.9 KHz.

If the desired cut-off frequency is specified, the cut-off particle size below which the seed particle responds to the fluid velocity well can be easily determined as

$$a_{\text{cut-off}} \approx \varepsilon_{\text{cut-off}}\sqrt{\pi f_{\text{cut-off}}/\nu} \quad (26)$$

where $\varepsilon_{\text{cut-off}}$ is estimated from Eq. (24) for a given particle-to-fluid density ratio.

4 Particle response to isotropic turbulence

Complex flows often possess a wide range of length scale and time scale. Thus, it may be insufficient to just use one criterion in the outset to determine the cut-off particle size $a_{\text{cut-off}}$ in measuring the statistics of inherently unsteady, nonuniform flows unless the highest cut-off frequency is specified. We consider the response of the seed particle to isotropic turbulence as an example. In using PIV or HPIV to measure an instantaneous turbulent flow, one is interested in capturing the large scale structure, turbulence energy, Taylor micro-scale structure, and/or even Kolmogorov length scale structure if the seed particle density is high. In an LDV measurement of turbulent flows field, it is typically required that seed particles respond well to the velocity fluctuation in the energy containing range so that turbulence intensity of the fluid can be represented by that of the seed particles. For example, fluid turbulence energy spectra were obtained in a solid–gas suspension flow using LDV (Tsuji et al. 1984) which requires a good response of the seed particles to all wave number components.

4.1 Particle diffusivity, turbulent intensity, and the second invariant

Based on the studies on the particle dispersion in turbulence (Taylor 1921; Reeks 1977), it is known that the long-time particle diffusivity is controlled by the large scale structure,

$$D_{\alpha\alpha} = \int_0^\infty R_{v_\alpha v_\alpha}(\tau)\,\mathrm{d}\tau = \frac{1}{\pi} S_{v_\alpha v_\alpha}(\omega=0), \quad \alpha=1, 2, \text{ or } 3 \quad (27)$$

where $R_{v_i v_j}(\tau)$ and $S_{v_i v_j}(\omega)$ are the Lagrangian correlation tensor and power spectrum tensor of the particle velocity fluctuation. For particle diffusivity $D_{\alpha\alpha}$ to represent accurately the fluid diffusivity D_f, only the low-frequency range of the Lagrangian fluid velocity needs to be accurately represented. The particle turbulence intensity (i.e. the mean square value of the particle velocity fluctuation) is dictated by the energy containing range of the fluid turbulence spectrum,

$$\langle v_\alpha^2 \rangle = R_{v_\alpha v_\alpha}(\tau=0) = \int_0^\infty S_{v_\alpha v_\alpha}(\omega)\,\mathrm{d}\omega \quad (28)$$

where $\langle\ \rangle$ denotes ensemble average. For the turbulence intensity $\langle v_\alpha^2\rangle$ of the seed particle to represent accurately the fluid turbulence intensity, u_0^2, almost the entire Lagrangian power spectrum of the fluid turbulence needs to be faithfully followed by the seed particle.

Turbulent flow is full of intense vortical regions and high strain-rate stagnation regions. Let us consider the second invariant of the turbulence deformation tensor,

$$\mathrm{II}_d = -\frac{1}{2}\frac{\partial u_i}{\partial x_j}\frac{\partial u_j}{\partial x_i} = -(S^2 - \Omega_j\Omega_j/4)/2, \quad (29)$$

where $S=(s_{ij}s_{ji})^{1/2}$ is the Euclidean norm of the strain-rate tensor $s_{ij}=(\partial u_i/\partial x_j + \partial u_j/\partial x_i)/2$, Ω_j is the jth component of the vorticity, and $\Omega^2=\Omega_j\Omega_j$ is the enstrophy. For homogeneous turbulence, it can be shown (Hinze 1975; p. 347) that

$$\langle \mathrm{II}_d \rangle = 0 \quad (30)$$

so that

$$\langle S^2 \rangle = \tfrac{1}{4}\langle \Omega_j\Omega_j \rangle. \quad (31)$$

However, for seed particles with finite inertia, the trajectories are biased either toward intense vortical regions for bubbles or high strain rate stagnation regions for heavy particles (Maxey 1987; Squire and Eaton 1990; Tio et al. 1993; Wang and Maxey 1993; Mei 1993). Denote $S_p(t;\beta)$ and $\Omega_p^2(t;\beta)$ as the respective Euclidean norm of s_{ij} and the enstrophy of the fluid turbulence seen by the particle with finite β at a given instant t. It is noted that the time averaged or ensemble averaged value $\langle S_p^2(\beta)\rangle$ is different from that of fluid, $\langle S^2\rangle$. Only for inertialess particle, $\langle S_p^2(\beta\to\infty)\rangle = \langle S^2\rangle$. It is observed in Monte-Carlo simulations (see Sect. 4.2) that $\langle S_p^2(\beta)\rangle$ and $\langle \Omega_p^2(\beta)\rangle/4$ of finite inertia deviate from $\langle S^2\rangle$ similarly, but in opposite directions as the particle inertia β^{-1} increases. Thus one may use $1-\langle S^2(\beta)\rangle/\langle S^2\rangle$ or simply combine the biases in S^2 and Ω^2 to define a dimensionless number

$$r = -\frac{\langle S_p^2(\beta)\rangle - \langle \Omega_p^2(\beta)\rangle/4}{\langle S^2\rangle} = \frac{2\langle \mathrm{II}_d(\beta)\rangle}{\langle S^2\rangle} \quad (32)$$

that is useful to measure the bias in the sampling of vortical and stagnation regions by seed particles. It is noted that $r \to 0$ as particle inertia β^{-1} goes to zero, which is the ideal case. A larger value of r, or $\langle II_d \rangle$, implies a more non-uniform instantaneous spatial distribution of particle concentration (Maxey 1987). In Wang and Maxey (1993), the connection between the particle concentration and the enstrophy $\langle \Omega^2 \rangle$, hence r, was shown clearly. The extent to which non-uniform particle concentration affects particle-based fluid velocity measurements depends directly on the magnitude of r and the quantity of interest. Systematic bias is observed in the particle settling velocity due to increasing values of r (Maxey 1987; Wang and Maxey 1993; Mei 1993). If the fluid vorticity is of interest and heavier seed particles are used, the result may be biased to give lower vorticity since the particle concentration is lower in the vortical regions. The dimensionless value of r thus provides a convenient measure of the statistical bias towards the vortical or stagnation regions. One may consider $r \sim 0.1$ to be quite undesirable since it represents a 10% bias, in the mean square sense, in the sampling of the vortical and stagnation regions by the seed particles. Since $\langle II_d \rangle$ involves the statistics of the spatial derivatives of the velocity, $\langle II_d \rangle$ clearly scales by u_0^2/λ^2 in which λ is the Taylor micro-length scale. Thus, r measures the fidelity of the particle in tracking the Taylor micro-length scale structure. This scaling is also easily seen from the definition of II_d in Eq. (29).

It is also noted that λ/u_0 gives the Kolmogorov time scale

$$\tau_K = \frac{1}{\sqrt{15}} \frac{\lambda}{u_0} \tag{33}$$

which is the relevant time scale used to describe the particle preferential concentration or particle trajectory bias in Wang and Maxey (1993). We will use $D_{\alpha\alpha}$, $\langle v_\alpha^2 \rangle$, and r to characterize the response of the speed particle to the integral length scale structures, to turbulence energy, and to the Taylor micro-length scale structure.

4.2 Turbulence energy spectrum and Monte-Carlo simulation

The following energy spectrum $E(k)$ (Mei and Adrian 1995) is used to describe the spatial structure of the turbulence,

$$E(k) = \frac{3}{2} u_0^2 \alpha \frac{k^4}{k_0^5} \frac{1}{[1+(k/k_0)^2]^{17/6}} \exp(-\eta_0^2 k^2) \tag{34}$$

where α is the normalizing coefficient, k_0 is a wave number typical of the energy containing range, and the parameter $\tilde{\eta}_0 = \eta_0 k_0$ is related to the turbulence Reynolds number Re_λ. Although an exponential cut-off for $E(k)$ in the viscous dissipation range has been observed at finite Re_λ (Comte-Bellot and Corrsin 1971; Yeung and Pope 1989; Domaradzki 1992 and and Wang and Maxey 1993), the Gaussian decay is adopted because an approximate relation between $\tilde{\eta}_0$ and Re_λ has been developed for the energy spectrum model described by (34) and the model has been used to study the dispersion of heavy particles (Mei and Adrian 1995). A composite form of the Eulerian turbulence power spectrum $\tilde{D}(\omega)$, which is the Fourier transformation of the Eulerian autocorrelation of the turbulence in the reference frame moving with the mean flow velocity, was constructed in Mei and Adrian (1995) to describe the temporal structure of the turbulence,

$$\tilde{D}(\omega) = \tilde{A} \frac{\exp(-\eta_1^2 \omega^2)}{1+(T\omega)^2} \tag{35}$$

where $\tilde{A}$ is determined by satisfying $\int_{-\infty}^{\infty} \tilde{D}(\omega)\, d\omega = 1$. The Eulerian integral time scale T_0, which is equal to $\pi\tilde{D}(0)$, is related to the integral length scale L_{11} as $T_0 = c^E L_{11}/u_0$. The relation between $k_0\eta_0$ and Re_λ, the dependence of c^E on Re_λ, the choice for η_1, the relation between T and T_0, and the results on the dispersion of heavy particles using the above $E(k)$ and $\tilde{D}(\omega)$ can be found in Mei and Adrian (1995).

To study the response of seed particles to turbulent liquid flow, a random, isotropic, Gaussian, pseudo-turbulence is simulated. The velocity is represented as

$$u_i(\mathbf{x}, t) = \sum_{m=1}^{N} [b_i^{(m)} \cos(\mathbf{k}^{(m)} \cdot \mathbf{x} + \omega^{(m)} t) + c_i^{(m)} \sin(\mathbf{k}^{(m)} \cdot \mathbf{x} + \omega^{(m)} t)] \tag{36}$$

where N (=128 in this study) is the number of the Fourier modes, and $\mathbf{k}^{(m)}$ and $\omega^{(m)}$ are the wave number and frequency of the m-th mode. Without loss of generality in the Monte-Carlo simulation, k_0 is set to one. The random wave number $\mathbf{k}^{(m)}$ is chosen to follow an algebraically decaying probability density function (pdf) as

$$p_{1i}(k_i) = \frac{\zeta-1}{2}(1+|k_{1i}|)^{-\zeta} \quad \text{for } i = 1, 2, \text{ or } 3. \tag{37}$$

In this study, $\zeta = 1.2$ is used to allow $p_{1i}(k_i)$ to decay slowly so that the high k components are sampled sufficiently. This slow decay of $p_{1i}(k_i)$ is important to ensure convergence of the high-order statistics such as $\langle II_d \rangle$ and $\langle S^2 \rangle$ at high Re_λ. The random frequency $\omega^{(m)}$ is chosen according to the following pdf

$$p_2(\omega) = \frac{1}{\pi} \frac{1}{1+(\omega/\omega_0)^2} \tag{38}$$

where

$$\omega_0 = \sqrt{2\pi} u_0 / L_{11} \tag{39}$$

is a typical frequency. The random coefficients $b_i^{(m)}$ and $c_i^{(m)}$ follow a normal distribution and are scaled to satisfy $E(k)$ and $\tilde{D}(\omega)$. The rest of the implementation details can be found in Maxey (1987) and Mei (1990). The simulation results are based on ensemble averages over 4000–10 000 particles.

Equation (8) in vector form can be made dimensionless by introducing

$$t^* = t\omega_0, \quad \omega^* = \omega/\omega_0, \quad \mathbf{x}^* = \mathbf{x}\sqrt{2\pi}/L_{11}, \quad \mathbf{u}^* = \mathbf{u}/u_0, \quad \mathbf{V}^* = \mathbf{V}/u_0, \quad \mathbf{k}^* = \mathbf{k}L_{11}/\sqrt{2\pi}. \tag{40}$$

Neglecting the gravitational force for simplicity, the resulting equation is

$$\frac{d\mathbf{V}^*}{dt^*} = \beta_S \left[\phi(\mathbf{u}^* - \mathbf{V}^*) + \varepsilon_0 \int_0^{t^*} K(t^* - \tau^*) \frac{d(\mathbf{u}^* - \mathbf{V}^*)}{d\tau^*} d\tau^* \right] + \frac{3}{2} \frac{1}{\rho + 1/2} \frac{D\mathbf{u}^*}{Dt^*}. \tag{41}$$

The particle displacement is obtained from

$$\frac{d\mathbf{y}^*}{dt^*}=\mathbf{V}^*. \tag{42}$$

The initial conditions are

$$\mathbf{y}^*(0)=0, \quad \mathbf{V}^*(0)=\mathbf{u}^*(\mathbf{x}=0, t=0). \tag{43}$$

In Eq. (41),

$$\beta_S=9\nu/[2(\rho+1/2)a^2\omega_0], \tag{44}$$

$$\varepsilon_0=(a^2\omega_0/2\nu)^{1/2}=\frac{3}{2}[\beta_S(\rho+1/2)]^{-1/2} \tag{45}$$

are the dimensionless particle inertia parameter and the Stokes number. The particle diffusivity is normalized by $u_0L_{11}/\sqrt{2\pi}$, the particle turbulence intensity by u_0^2, and $\langle \mathrm{II}_d \rangle$ by λ^2/u_0^2. In presenting the results, the following dimensionless inertia parameter based on the Kolmogorov time scale,

$$\beta_K=\beta\tau_K, \tag{46}$$

will be used, following Wang and Maxey (1993). Hereinafter, the superscript "*" will be omitted for convenience. The equation of motion is integrated with second order accuracy. The evaluation of the history force is similar to that of Reeks and Mckee (1984). For simplicity, we restrict the discussion to fine particles so that particle Reynolds number is very small. For solid particles in gas flow, the results of the analytical study (Mei and Adrian 1995) using Eqs. (34–35) and independence approximation will be examined and re-interpreted.

4.3
Discussion

Figures 3 and 4 show the diffusivity, D_{22}, and turbulence intensity, $\langle v_2^2 \rangle$, of contaminated micro-bubbles over a large range of particle inertia in isotropic turbulence with $Re_\lambda=53.5$. Monte-Carlo simulations with and without the history force (F_H) are carried out. The inclusion of F_H increases the inertia of the bubble and thus reduces D_{22} and $\langle v_2^2 \rangle$ of large size bubble.

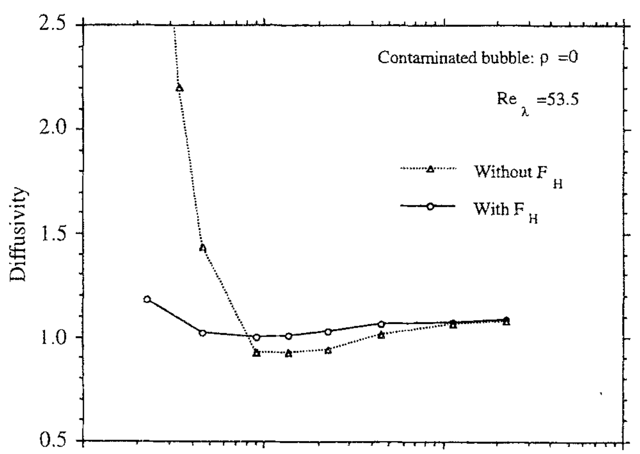

Fig. 3. Turbulent diffusivity of contaminated micro bubble as a function of $\beta\tau_K$ at $Re_\lambda=53.5$

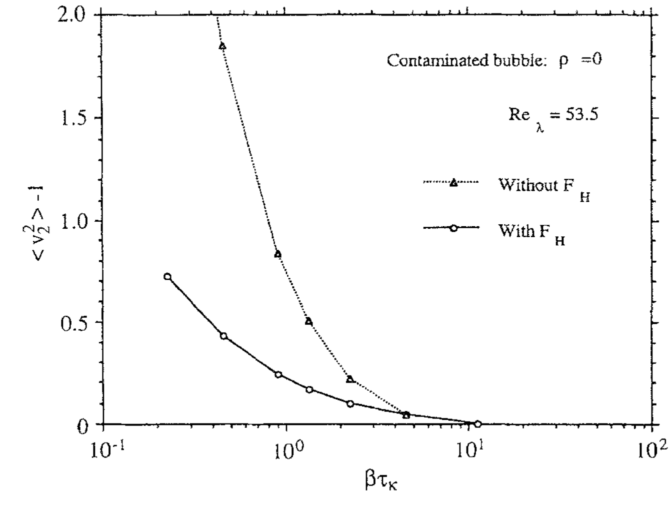

Fig. 4. Turbulent intensity of contaminated micro bubble, $\langle v^2 \rangle - 1$, as a function of $\beta\tau_K$ at $Re_\lambda=53.5$

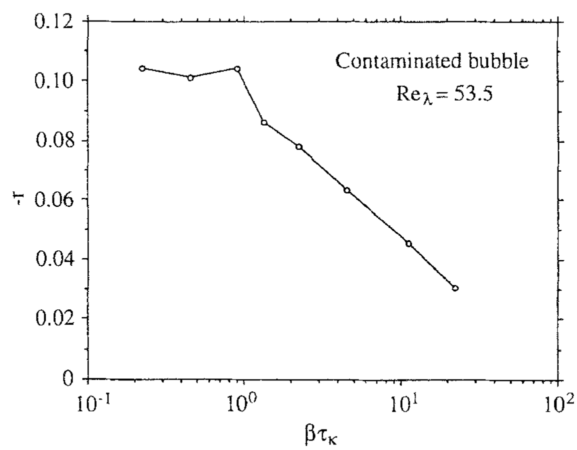

Fig. 5. Ratio of the second invariant to the magnitude of the strain rate tensor, $r=2\langle \mathrm{II}_d \rangle / S_\infty^2$, evaluated on the trajectory of contaminated micro bubble as a function of $\beta\tau_K$ at $Re_\lambda=53.5$

With F_H included (which is more realistic), D_{22} is insensitive to the inertia over a large range of $\beta\tau_K$. The turbulence intensity $\langle v_2^2 \rangle$ approaches unity only after $\beta\tau_K$ exceeds 10. Hence $\langle v_2^2 \rangle$ is a more stringent measure for seed particle fidelity. Since the diffusivity of solid particle is not sensitive to β in general, it is clear that $D_{\alpha\alpha}$ is not a good quantity to gauge the fidelity of the seed particle. The behavior of diffusivity or the fidelity on the integral length scale will not be discussed further.

Figure 5 shows the variation of $-r$ as a function of $\beta\tau_K$. With $\beta\tau_K<1$, r is close to be -10%. It was observed that as particle inertia increases, $\langle S_p^2(\beta) \rangle$ and $\langle \Omega_p^2(\beta) \rangle/4$ deviate from the fluid value $\langle S^2 \rangle$ similarly but in opposite directions. Since $r<0$, the bubbles sample more frequently the vortical regions than the stagnation region because they tend to accumulate in the vortical region. Clearly, it takes even larger values of $\beta\tau_K$ (cf. last paragraph) to reduce the trajectory bias of the seed particle on the Taylor micro-length scale.

Figure 6 shows the energy loss of the heavy particle, $e_{\mathrm{loss}}=1-\langle v_2^2 \rangle$, as a function of $\beta\tau_K$ for $Re_\lambda=40.6$, 53.5, 124.4,

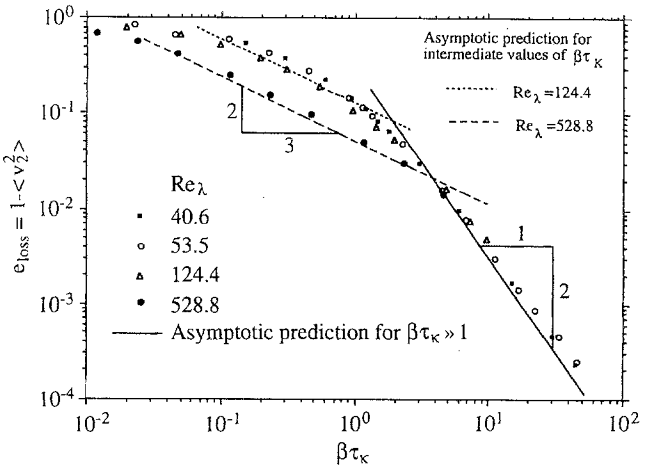

Fig. 6. Turbulent intensity, $1-\langle v^2\rangle$, of solid particle ($\rho_p/\rho_f\to\infty$) as a function of $\beta\tau_K$ at various values of Re_λ

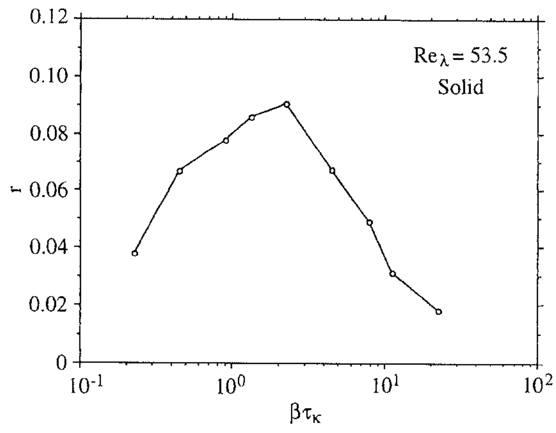

Fig. 7. $r=2\langle \mathrm{II}_d\rangle/\langle S^2\rangle$ on the trajectory of solid particle ($\rho_p/\rho_f\to\infty$) as a function of $\beta\tau_K$ at $Re_\lambda=53.5$

and 528.8 (corresponding to $\eta_0 k_0=0.1$, 0.05, 0.01, and 0.001). The results are obtained using the method developed in Mei and Adrian (1995) for heavy particles with the unsteady forces neglected. Since $\langle v_2^2\rangle$ is obtained by carrying out numerical integration, the numerical accuracy in e_{loss} is low for $Re_\lambda=124.4$ and 528.8 with large value of $\beta\tau_K$. Two different asymptotes for e_{loss} in different ranges of $\beta\tau_K$ are obtained in this study; details are given in the Appendix. For intermediate values of $\beta\tau_K$, $e_{\mathrm{loss}}\sim O((\beta\tau_K)^{-2/3})$. For $Re_\lambda\geqslant 40$ and $\beta\tau_K>2.5$, Fig. 6 shows that e_{loss} scales with $\beta\tau_K$ and the asymptotic behavior of the particle energy loss (see the derivations leading to Eq. (A17)) is given by

$$e_{\mathrm{loss}}\sim 0.3127(\beta\tau_K)^{-2} \qquad (47)$$

to the leading order. Even better agreement between the asymptotic prediction and numerical integration can be obtained if (A16), which includes the next-order term, is used for finite values of $\eta_0 k_0(<1)$. Since Eq. (47) is for all Re_λ ($\geqslant 40$), it is thus useful for practical purpose. It may be used for heavy, fine particles with $e_{\mathrm{loss}}<5\%$ or $\beta\tau_K>2.5$.

Suppose one desires to select the seed particle in a gas flow with 95% or more energy captured by the seed particle. The above asymptotic relation and Eq. (20) give the required particle size if τ_K is known and ρ is specified,

$$a<2.84 e_{\mathrm{loss}}^{1/4}\sqrt{\frac{\nu\tau_K}{\rho+0.5}} \quad \text{for } e_{\mathrm{loss}}<0.05. \qquad (48)$$

This result is not just limited to isotropic turbulence. For anisotropic turbulence, the anisotropy is usually on large scales to which the seed particles can easily respond. Hence the small-scale isotropy approximation can be invoked, and Eqs. (47–48) can be applied to estimate the energy loss or the desired cut-off size of the seed particle.

Figure 7 shows the dependence of $r=2\langle \mathrm{II}_d\rangle/\langle S^2\rangle$ on $\beta\tau_K$ for solid particle at $Re_\lambda=53.5$. The result is obtained from the Monte-Carlo simulation outlined in Sect. 4.2. It is seen that trajectory bias for solid particle peaks around $\beta\tau_K=2.3$, which is in qualitative agreement with the observation made by Wang and Maxey (1993) that the particle preferential concentration maximizes near $\beta\tau_K=1$. Similar to Fig. 5, $\langle \mathrm{II}_d\rangle$ decreases slowly with increasing $\beta\tau_K$. Even for $\beta\tau_K=8.7$, r is around 5% while e_{loss} is only 0.4% based on (47). While the energy loss on this order of magnitude may be acceptable for an LDV measurement, $r\sim 5\%$ may produce a noticeable micro-scale non-uniform concentration which biases the measurements toward higher strain-rate stagnation regions. One should also note that due to the Gaussian decay of $E(k)$ in (34) and the neglect of the triple correlation in the turbulence in (36), the present simulation may have already under-predicted the trajectory bias (cf. Wang and Maxey 1993). How this level of trajectory bias affects the overall measurement errors of the vorticity field is not clear at this stage, and should be the subject of further studies.

As seen from Fig. 1, particle response improves with decreasing density ratio ρ for $\rho>1$. For solid particles in liquid, the effect of the unsteady forces is clearly important. Hence, Monte-Carlo simulation is carried out to investigate the response of seed particles. Figure 8 shows $\langle v_2^2\rangle$ at $\beta\tau_K=2.254$, $Re_\lambda=53.5$ over a large range of density ratio ρ. Clearly, the best response is achieved near $\rho=1$ as expected. On the other hand, since $\langle v_2^2\rangle$ does not change much for $\rho>2.5$, one may use Eqs. (20) and (47) to estimate the required particle size for

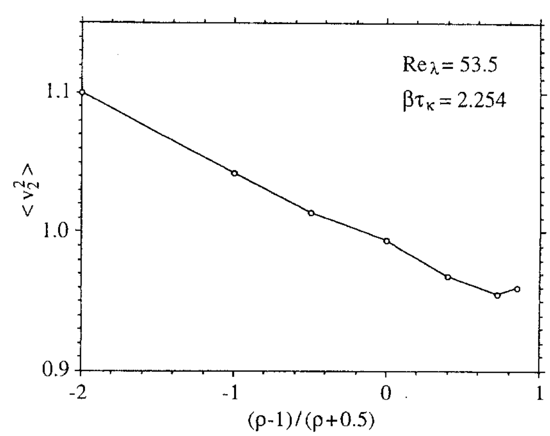

Fig. 8. Particle turbulent intensity $\langle v_2^2\rangle$ as a function of $(\rho-1)/(\rho+1/2)$ at $\beta\tau_K=2.254$

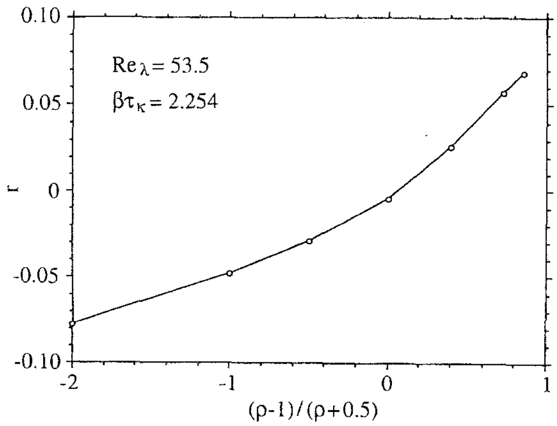

Fig. 9. Variation of $r=2\langle \mathrm{II}_d\rangle/\langle S^2\rangle$ evaluated on the trajectory of a particle as a function of $(\rho-1)/(\rho+1/2)$ at $\beta\tau_K=2.254$, $Re_\lambda=53.5$

a given energy loss. Of course, if neutrally buoyant particles are used, better velocity fidelity will be achieved. Figure 9 shows r over a wide range of ρ under the same condition. The bias in the particle trajectory vanishes as ρ approaches 1.

In summary, one needs to use large values of β to reduce $\langle \mathrm{II}_d\rangle$ and e_{loss} for solid particle in gas flow. One needs to use large β and near unity ρ to effectively eliminate $\langle \mathrm{II}_d\rangle$ and e_{loss} for solid particles in liquid.

Appendix

Asymptotic behavior of the energy loss of heavy fine particles

The intensity of turbulent fluctuation of heavy particles can be evaluated as

$$\langle v_2^2\rangle=\beta\int_0^\infty \exp(-\beta\tau)R_{uu}^p(\tau)\,\mathrm{d}\tau \tag{A1}$$

(Mei 1990) where $R_{uu}^p(\tau)$ is the fluid velocity correlation evaluated on the particle trajectory. Defining

$$\bar{t}=tk_0u_0,\quad \bar{\omega}=\omega/k_0u_0,\quad \bar{\mathbf{x}}=\mathbf{x}k_0,\quad \mathbf{u}^*=\mathbf{u}/u_0,$$
$$\mathbf{v}^*=\mathbf{v}/u_0,\quad \bar{\mathbf{k}}=\mathbf{k}/k_0 \tag{A2}$$

where k_0 is the same typical wave number appearing in Eq. (34), it is easy to show in the large $\bar{\beta}$ limit that if

$$\bar{R}_{uu}^p(\bar{\tau})\sim 1-c\bar{\tau}^b\quad \text{for } \bar{\tau}\ll 1, \tag{A3}$$

(A1) gives

$$\langle v_2^2\rangle\sim 1-c\Gamma(b+1)\bar{\beta}^{-b} \tag{A4}$$

where $\Gamma(x)$ is the Gamma function. Mei and Adrian (1995) have shown using independence approximation for heavy particles in isotropic turbulence whose energy spectrum is described by (34) with *zero settling velocity* that

$$\bar{R}_{uu}^p(\bar{\tau})=\frac{\alpha(\bar{\eta}_0)\bar{D}(\bar{\tau})}{\alpha\{[\bar{\eta}_0^2+\frac{1}{2}\bar{Y}(\bar{\tau})]^{1/2}\}}. \tag{A5}$$

In dimensional forms, $D(\tau)$ is Eulerian auto-correlation whose Fourier transformation is given by (35) and $Y(\tau)$ is the mean square particle displacement which can be evaluated, in dimensionless form, as

$$\bar{Y}(\bar{\tau})=2\int_0^{\bar{\tau}}(\bar{\tau}-t')\bar{R}_{vv}(t')\,\mathrm{d}t'. \tag{A6}$$

To gain an insight on the dependence of e_{loss} on particle inertia and turbulence structure, we consider the following limits,

$$\bar{\eta}_0\ll 1 \tag{A7}$$

and

$$\bar{\beta}=\beta k_0u_0\gg 1. \tag{A8}$$

Under the condition $\bar{\beta}\gg 1$, $\langle v_2^2\rangle\sim 1$ to the leading order so that

$$\bar{Y}(\bar{\tau})\sim\tfrac{1}{2}\bar{\tau}^2\quad \text{for } \bar{\tau}\ll 1. \tag{A9}$$

Mei (1990) has derived for $\bar{\eta}_0\ll 1$ that

$$\alpha^{-1}(\bar{\eta}_0)\sim 1.0325-2.0311\bar{\eta}_0^{2/3}. \tag{A10}$$

For very small $\bar{\tau}$, the Eulerian auto-correlation can be expressed as

$$\bar{D}(\bar{\tau})\sim 1-\tfrac{1}{2}\bar{\tau}^2/\bar{\tau}_\lambda^2 \tag{A11}$$

where $\bar{\tau}_\lambda$ is the Eulerian Taylor micro-time scale of the turbulence and is given by

$$\bar{\tau}_\lambda^2\sim\sqrt{\pi\bar{\eta}_0\bar{T}_0}\quad \text{for } \bar{\eta}_0\ll 1. \tag{A12}$$

In Eq. (A5),

$$\alpha^{-1}\{[\bar{\eta}_0^2+\tfrac{1}{2}\bar{Y}(\bar{\tau})]^{1/2}\}\sim 1.0325-2.0311\,[\bar{\eta}_0^2+\tfrac{1}{2}\bar{Y}(\bar{\tau})]^{1/3}$$
$$\sim 1.0325-2.0311\,[\bar{\eta}_0^2+\tfrac{1}{2}\bar{\tau}^2]^{1/3} \tag{A13}$$

for small values of $[\bar{\eta}_0^2+\frac{1}{2}\bar{Y}(\bar{\tau})]^{1/2}$ and $\bar{\tau}^2$. Two different expansions for $[\bar{\eta}_0^2+\frac{1}{2}\bar{Y}(\bar{\tau})]^{1/3}$ are possible:

i) $\bar{\beta}\gg\bar{\eta}_0^{-1}\gg 1$ so that $[\bar{\eta}_0^2+\frac{1}{2}\bar{\tau}^2]^{1/3}\sim\bar{\eta}_0^{2/3}+\frac{1}{6}\bar{\tau}^2\bar{\eta}_0^{-4/3}$

$$\text{for } \bar{\tau}\ll\bar{\beta}^{-1}\ll\bar{\eta}_0 \tag{A14}$$

and

ii) $\bar{\eta}_0^{-1}\gg\bar{\beta}\gg 1$ so that $[\bar{\eta}_0^2+\frac{1}{2}\bar{\tau}^2]^{1/3}\sim\frac{1}{2^{1/3}}\bar{\tau}^{2/3}$

$$\text{for } \bar{\eta}_0\ll\bar{\tau}\ll\bar{\beta}^{-1}. \tag{A15}$$

For the first case, $\bar{\beta}\gg\bar{\eta}_0^{-1}\gg 1$, Eqs. (A4–A5) give

$$e_{\mathrm{loss}}=1-\langle v_2^2\rangle/u_0^2\sim 0.6557(\bar{\beta}^{-2}\bar{\eta}_0^{-4/3})+(\bar{\beta}\bar{\tau}_\lambda)^{-2}.$$

Noting $\bar{\tau}_K\sim\frac{1}{\sqrt{15}}2.6744\bar{\eta}_0^{2/3}=0.6905\bar{\eta}_0^{2/3}$ for $E(k)$ given by (34), the above becomes

$$e_{\mathrm{loss}}\sim 0.3127(\beta\tau_K)^{-2}+(\sqrt{\pi\bar{\eta}_0\bar{T}_0}\bar{\beta}^2)^{-1}=0.3127(\beta\tau_K)^{-2}$$
$$+0.3237\frac{\bar{\tau}_K^{1/2}}{c^E\bar{T}_0}(\bar{\beta}\bar{\tau}_k)^{-2}$$
$$=0.3127(\beta\tau_K)^{-2}[1+1.04\bar{\tau}_K^{1/2}/(c^E\bar{T}_0)]. \tag{A16}$$

To the leading order, e_{loss} is given by

$$e_{\mathrm{loss}}\sim 0.3127(\beta\tau_K)^{-2}\quad \text{for } \beta\tau_K\gg 1. \tag{A17}$$

For the second case, $\bar{\eta}_0^{-1} \gg \bar{\beta} \gg 1$, Eqs. (A4–A5) lead to

$$e_{\text{loss}} \sim \frac{2.0311}{1.0325} \frac{\Gamma(5/3)}{2^{1/3}} \bar{\beta}^{-2/3} + (\bar{\beta}\bar{\tau}_\lambda)^{-2}$$

$$\sim 1.41 (\tau_K k_0 u_0)^{2/3} (\beta\tau_K)^{-2/3} \tag{A18}$$

or

$$e_{\text{loss}} \sim 1.1 \bar{\eta}_0^{4/9} (\beta\tau_K)^{-2/3}. \tag{A19}$$

For predicting the energy loss of seed particles, Eq. (A17) is more appropriate since (A18) is only valid in a limited range of $\bar{\beta}$.

It is interesting to note that both Eqs. (A16) and (A18) indicate that the leading order terms of the energy loss for heavy fine particles result from its inability to follow the motion associated with the fine spatial turbulence structure on the Kolmogorov length scale. Another word, the origin of first term in e_{loss} can be traced back to the decay of $\alpha^{-1}\{[\bar{\eta}_0^2 + \frac{1}{2}\bar{Y}(\bar{\tau})]^{1/2}\}$ which is related to the spatial structure. The inability of the particle to follow the motion on the Taylor micro-time scale only contributes to higher order terms in (A16) and (A18) in the energy loss since $\bar{D}(\bar{\tau})$, which appears in Eq. (A5) for the correlation $\bar{R}^p_{uu}(\bar{\tau})$, decays at a slower rate near $\bar{\tau}=0$. If $E(k)$ with an exponential decay at high wave number is used, there will be a quantitative difference in the coefficient in Eq. (A17); but e_{loss} shall still scale with $\beta\tau_K$ for small inertia.

References

Adrian RJ (1991) Particle-imaging techniques for experimental fluid mechanics. Ann Rev Fluid Mech 23: 261–304

Auton TR; Hunt JCR; Prud'homme M (1988) The force exerted on a body in inviscid unsteady non-uniform rotational flow. J Fluid Mech 197: 241–257

Basset AB (1888) A Treatise on Hydrodynamics. Vol. 2, Dover Publications Inc.

Brabston Jr DC (1974) Numerical-solutions of steady viscous flow past sphere and gas bubbles. II. Numérical-solutions of singular end-point boundary-value. PhD thesis, California Institute of Technology

Chang E; Maxey MR (1995) Unsteady flow about a sphere at low to moderate Reynolds number. Part I. Oscillatory motion. J Fluid Mech 277: 347–379

Chang E; Maxey MR (1995) Unsteady flow about a sphere at low to moderate Reynolds number. Part II. Accelerated Motion. J Fluid Mech 303: 133–153

Chen JLS (1974) Growth of the boundary layer on a spherical gas bubble. J Appl Mech 41: 873–878

Cherukat P; McLaughlin JB; Dandy DS (1995) A computational study of the inertial lift on a sphere in a linear shear flow field. J Fluid Mech, submitted

Clift R; Grace JR; Weber ME (1978) Bubbles, drops and particles. Academic Press, New York

Comte-Bellot G; Corrsin S (1971) Simple Eulrerian time correlation of full- and narrow-band velocity signals in grid-generated, 'isotropic' turbulence. J Fluid Mech 48: 273–337

Dandy DS; Dwyer HA (1990) A sphere in shear flow at finite Reynolds number: effect of shear on particle lift, drag, and heat transfer. J Fluid Mech 216: 381–410

Domaradzki JA (1992) Nonlocal triad interactions and the dissipation range of isotropic turbulence. Phys Fluids A4(9): 2037–2045

Drew DA; Lahey Jr RT (1990) Some supplement analysis concerning the virtual mass and lift force on a sphere in a rotating and straining flow. Int J Multiphase Flow 16: 1127–30

Hinze JO (1975) Turbulence, McGraw-Hill, New York

Kim S; Karrila S (1991) Microhydrodynamics principles and selected applications. Butterworth-Heinmann Series in Chemical Engineering

Kim I; Pearlstein AJ (1990) Stability of the flow past a sphere. J Fluid Mech 211: 73–93

Kranfilian SK; Kotas TJ (1978) Drag on a sphere in unsteady motion in a liquid at rest. J Fluid Mech 87: 88–96

Lawrence CJ; Mei R (1995) Long-time behavior of the drag on a body in impulsive motion. J Fluid Mech 283: 307–327

Linteris GT; Libby PA; Williams FA (1991) Droplet dynamics in a non-uniform field. Combust Sci Tech 80: 319–335

Lovalenti PM; Brady JF (1993a) The hydrodynamic force on a rigid particle undergoing arbitrarily time-dependent motion at small Reynolds number. J Fluid Mech 256: 561–605

Lovalenti PM; Brady JF (1993b) The force on a bubble, drop, or particle in arbitrary time-dependent motion at a small Reynolds number. Phy Fluids A5 (9): 2104–16

Lovalenti P; Brady J (1995) The temporal behavior of the hydrodynamic force on a body in response to an abrupt change in velocity at small but finite Reynolds-number. J Fluid Mech 293: 35–46

Maxey MR (1987) The gravitational settling of aerosol particles in homogeneous turbulence and random flow fields. J Fluid Mech 174: 441–465

Maxey MR; Riley JJ (1983) Equation of motion for a small rigid sphere in a nonuniform flow. Phys Fluids 26 (4): 863–889

McLaughlin JB (1991) Inertial migration of a small sphere in linear shear flows. J Fluid Mech 224: 262–272

Mei R (1990) Particle dispersion in isotropic turbulence and unsteady particle dynamics at finite Reynolds number. Ph.D Thesis, University of Illinois at Urbana-Champaign, Urbana, IL

Mei R (1993) History force on a sphere due to a step change in the free-stream velocity. Int J Multiphase Flow 19(3): 509–525

Mei R (1994) Flow due to an oscillating sphere and an expression for unsteady drag on the sphere at finite Reynolds number. J Fluid Mech 270: 133–174

Mei R; Adrian RJ (1992) Flow past a sphere with an oscillation in the free-stream velocity and unsteady drag at finite Reynolds number. J Fluid Mech 237: 323–341

Mei R; Adrian RJ (1995) Effect of Reynolds number on isotropic turbulent dispersion. ASME J Fluids Eng 117(3): 402–409

Mei R; Klausner JF (1994) Shear lift force on spherical bubbles. Int J Heat Fluid Flow 15(1): 62–65

Mei R; Lawrence CJ (1996) The flow field due to a body in impulsive motion. To appear in J Fluid Mech

Mei R; Lawrence CJ; Adrian RJ (1991) Unsteady drag on a sphere at finite Reynolds number with small fluctuations in the free-stream velocity. J Fluid Mech 233: 613–628

Mei R; Klausner JF; Lawrence CJ (1994) A note on the history force on a spherical bubble at finite Reynolds number. Physics of Fluids A: Fluid Dynamics, 6(1), 418–420

Moorman RW (1955) Motion of a spherical particle in the accelerated portion of free fall. Ph.D Thesis, University of Iowa, Iowa

Odar F (1966) Verification of the proposed equation for calculation of the forces on a sphere accelerating in a viscous fluid. J Fluid Mech 25: 591–592

Odar F; Hamilton WS (1964) Forces on a sphere accelerating in a viscous fluid. J Fluid Mech 18: 302–314

Park WC; Klausner JF; Mei R (1995) Unsteady forces on spherical bubbles. Exp Fluids 19: 167–172; (1996) Erratum. Exp Fluids 21: 70

Reeks MW (1977) On the dispersion of small particles suspended in an isotropic turbulent fluid. J Fluid Mech 83: 529–546

Reeks MW; Mckee S (1984) The dispersive effects of Basset history forces on particle motion in a turbulent flow. Phys Fluids 27(7): 1573–82

Rivero M; Magnaudet J; Farbe, J (1991) New results on the forces exerted on a spherical body by an accelerated flow. C. R. Acad. Sci. Paris, 312, Série II, 1499–1506

Rubinow ST; Keller JB (1961) The transverse force on a spinning sphere moving in a viscous fluid. J Fluid Mech 11: 447–459

Saffman PG (1965) The lift on a small sphere in a slow shear flow. J Fluid Mech 22: 385–400

Saffman PG (1968) Corrigendum to: The lift on a small sphere in a slow shear flow. J Fluid Mech 31: 624

Sano T (1981) Unsteady flow past a sphere at low Reynolds number. J Fluid Mech 112: 433–441

Schöneborn P-R (1975) The interaction between a single particle and oscillating fluid. Int J Multiphase Flow 2: 307–317

Squires KD; Eaton JK (1990) Particle Response and Turbulence Modification in Isotropic Turbulence. Phys Fluids A 2(7): 1191–1203

Sridhar G; Katz J (1995) Drag and lift force on microscopic bubbles entrained by vortex. Phys Fluids 7(2): 389–399

Stokes GG (1851) On the effect of internal friction of fluids on the motion of pendulum. Trans. Camb. Phil. Soc. 9, 8. Reprinted in Math. and Phys. Papers III, Cambridge University Press, Cambridge (1992)

Sy F; Tauton JW; Lightfoot EN (1970) Transient creeping flow around sphere. AIChE J 16: 386–391

Taylor GI (1921) Diffusion by continuous movement. Proc Lond Math Soc Ser 2, 20, 196–211

Tchen CM (1947) Mean value and correlation problems connected with the motion of small particles suspended in a turbulent fluid. PhD thesis, Delft University, Netherlands

Tio KK; Ganan-Calvo AM; Lasheras JC (1993) The dynamics of small, heavy, rigid spherical particles in a periodic Stuart vortex flow. Phys Fluids 5(7): 1679–93

Torobin LB; Gauvin WH (1959) Fundamental aspects of solid gas flow. Part III. Can J Chem Eng 37: 224–236

Tsuji Y; Morikawa Y; Shiomi H (1984) LDV measurements of an air–solid two-phase flow in a vertical pipe. J Fluid Mech 139: 417–434

Tsuji Y; Morikawa Y; Mizuno O (1985) Experimental measurement of the Magnus forces on a rotating sphere at low Reynolds number. J Fluids Eng 107: 484

Tsuji Y; Kato N; Tanaka T (1991) Experiments on the unsteady drag and wake of a sphere at high Reynolds numbers. Int J Multiphase Flow 17(3): 343–354

Wang LP; Maxey MR (1993) Settling velocity and Concentration Distribution of Heavy Particles in Homogeneous Isotropic Turbulence. J Fluid Mech 256: 27–68

Yang SM; Leal LG (1991) A note on memory-integral contributions to the force on an accelerating spherical drop at low Reynolds number. Phys Fluids A 3(7): 1822–1824

Yeung PK; Pope SB (1989) Lagrangian statistics from Direct Numerical Simulations of Isotropic Turbulence. J Fluid Mech 207: 531–586